

Structural and Biochemical Characterization of the Cytochrome P450 CypX (CYP134A1) from *Bacillus subtilis*: A Cyclo-L-leucyl-L-leucyl Dipeptide Oxidase[†]

Max J. Cryle,^{*,‡} Stephen G. Bell,[§] and Ilme Schlichting[‡]

[‡]*Department of Biomolecular Mechanisms, Max Planck Institute for Medical Research, Jahnstrasse 29, 69120 Heidelberg, Germany, and* [§]*Department of Chemistry, Inorganic Chemistry Laboratory, University of Oxford, South Parks Road, Oxford OX1 3QR, U.K.*

Received June 7, 2010; Revised Manuscript Received July 27, 2010

ABSTRACT: Cytochrome P450 CypX (CYP134A1), isolated from *Bacillus subtilis*, has previously been implicated in the three-step oxidative transformation of the diketopiperazine cyclo-L-leucyl-L-leucyl into pulcherriminic acid, a precursor of the extracellular iron chelate pulcherrimin. In this study, we present the first experimental data relating to CYP134A1, where we show that CYP134A1 binds cyclo-L-leucyl-L-leucyl with an affinity of $24.5 \pm 0.5 \mu\text{M}$. Structurally related diketopiperazines sharing similar alkyl side chains to cyclo-L-leucyl-L-leucyl also bind to CYP134A1 with comparable affinity. CYP134A1 is capable of catalyzing the *in vitro* oxidation of diketopiperazine substrates when supported with several alternate electron transfer partner systems. Products containing one additional oxygen atom and which are intermediate products of the expected pulcherriminic acid were identified by GCMS. The oxidation of related diketopiperazines reveals that different oxidative pathways exist for CYP134A1-catalyzed diketopiperazine oxidation. The crystal structure of CYP134A1 has been determined to 2.7 Å resolution in the absence of substrate and in the presence of bound phenylimidazole ligands to 3.1 and 3.2 Å resolution. The active site is dominated by hydrophobic residues and contains an unusual proline residue in place of the normally conserved alcohol residue that typically plays an important role in oxygen activation. The B–B₂ substrate recognition loop, which forms part of the active site, shows considerable flexibility and was found in both open and closed conformations in different structures. These results represent the first insights into the structural and biochemical basis underlying the multistep oxidation catalyzed by CYP134A1.

The cytochromes P450 (P450s) are a superfamily of hemoproteins that catalyze a varied and impressive range of oxidative transformations in nature. The roles P450s play are highly variable and organism dependent, with plants and bacteria utilizing P450s widely in biosynthetic transformations in secondary metabolism, while mammals and humans utilize P450s in hormone biosynthesis and xenobiotic metabolism (1). The substrate specificity of P450s can be broad, for instance, in the case of xenobiotic metabolism, or tightly regulated, a situation that arises in natural product biosynthesis. The large number of different substrates that undergo oxidation by the P450 superfamily is made yet more impressive by the ability of P450s to catalyze a number of different oxidative reactions upon their substrates. These range from the archetypal P450 reaction, oxidation of unactivated C–H bonds, to aromatic hydroxylation, double bond epoxidation, heteroatom oxidation, and phenolic coupling (2). Multiple-step reactions catalyzed by a single P450 on a substrate are also well established and include carbon–carbon bond cleavage following prior oxidation of the cleavage site (2).

The mechanism of substrate oxidation by P450s has received significant attention, with many experimental approaches utilized to build a consensus picture of oxygen activation and substrate hydroxylation by P450s (3, 4). In contrast to alkane hydroxylation, relatively little is known about P450-catalyzed

heteroatom oxidation, in part due to the fewer instances of natural products known to undergo such P450-mediated oxidations. Studies of P450-catalyzed nitrogen oxidation have been performed largely with mammalian xenobiotic metabolizing P450s (5), the results of which have indicated that several mechanistic fates are possible (6). These include initial electron transfer from the nitrogen atom, followed by direct oxidation of the heteroatom or deprotonation of an adjacent carbon that can undergo recombination with the iron-tethered hydroxy radical. Elimination of this hydroxyl group can result in imine formation or dealkylation of the parent compound. Direct insertion of oxygen into the N–H bond is also possible, a process that results in the formation of a hydroxylamine. Examples of P450-catalyzed heteroatom oxidation in secondary metabolism occur in the biosynthesis of nocardicin A, a member of the monocyclic β -lactam antibiotics (7), and in the formation of oximes from various amino acids by members of the CYP79 and CYP83 subfamilies, where a sequential series of nitrogen oxidations form the product oxime from an initial amine (8–12).

Recently, the protein encoded by the *yvmC* gene from *Bacillus subtilis* has been shown to be a member of a newly described class of enzymes, the cyclodipeptide synthases (CDPs),¹ which catalyze

[†]M.J.C. is grateful for support of the International Human Frontier Science Program Organisation (Cross Disciplinary Fellowship).

*Address correspondence to this author. Telephone: +49 (6221) 486 516. Fax: +49 (6221) 486 585. E-mail: Max.Cryle@mpimf-heidelberg.mpg.de.

¹Abbreviations: CDP, cyclodipeptide synthase; cLL, cyclo-L-leucyl-L-leucyl; cYY, cyclo-L-tyrosyl-L-tyrosyl; cLF, cyclo-L-leucyl-L-phenylalanyl; cMM, cyclo-L-methionyl-L-methionyl; cAA, cyclo-L-alanyl-L-alanyl; cVV, cyclo-L-valyl-L-valyl; cLG, cyclo-L-leucyl-L-glycyl; cLP, cyclo-L-leucyl-L-prolyl; cLW, cyclo-L-leucyl-L-tryptophanyl; TFA, trifluoroacetic acid; SPE, solid phase extraction; GCMS, gas chromatography/mass spectrometry; rmsd, root mean square deviation; ACP, acyl carrier protein; TMSH, trimethylsulfonium hydroxide.

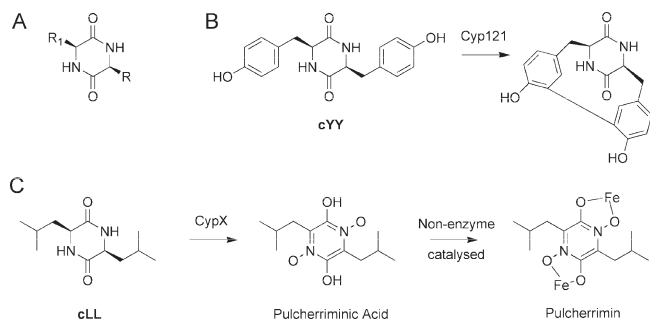


FIGURE 1: P450-mediated oxidation of dialkyldiketopiperazines. (A) General structure of dialkyldiketopiperazines, where R and R₁ are amino acid side chains. (B) The oxidation of cYY by the *M. tuberculosis* P450 CYP121. (C) The formation of pulcherriminic acid and pulcherrimin pigment from cLL involving the *B. subtilis* P450 CYP134A1.

the formation of cyclic dipeptides in a number of organisms (13). These enzymes utilize charged tRNAs as substrates and are capable of synthesizing the corresponding cyclic dipeptides (dialkyldiketopiperazines, Figure 1) in an ATP-dependent manner. Cyclodipeptide synthases are often identified in close proximity to cytochrome P450s (13). The product of *yvmC* when expressed in *Escherichia coli* has been identified as the cyclic dipeptide cyclo-L-leucyl-L-leucyl (cLL), with the role of this compound in *B. subtilis* suggested as being a precursor for pulcherrimin, by both biochemical studies and transcriptional profiling (Figure 1) (14, 15).

Pulcherrimin is a red extracellular pigment formed by a number of species of bacteria and some species of yeast after growth in media enriched in iron(III) (16–23). The best characterized pulcherrimin is that produced by *B. subtilis*, where it has been shown to be an iron chelate of pulcherriminic acid, a hydroxamic acid derivative of the cyclic dipeptide cLL, formed via a nonenzymic reaction between pulcherriminic acid and iron(III) in the extracellular medium (Figure 1) (14, 20, 24). The exact role of the pigment is unclear, with the potential function of such siderochromes including roles as antibiotics, acting in a similar manner as that seen for aspergillins and related compounds, or siderophores such as the mycobactins (25). The formation of pulcherriminic acid from cLL in *B. subtilis* has indicated a role for the product of the gene downstream of *yvmC*, *cypX*. This gene encodes a cytochrome P450 (known as CypX or CYP134A1), with the mechanism of oxidation of cLL catalyzed by this P450 being intriguing. The mechanism involves three oxidative transformations, requiring the diketopiperazine nitrogen atoms to be oxidized to the corresponding *N*-oxides, together with the aromatization of the diketopiperazine ring either via hydroxylation and elimination of water or directly via an electron transfer reaction. Previously, CYP134A1 has been shown to oxidize certain steroidal substrates, although the biological relevance of such substrates was unclear (26, 27).

Due to the lack of direct experimental evidence concerning the substrate, structure, and mechanism of CYP134A1, we set about the biochemical and structural characterization of this mechanistically distinct P450.

EXPERIMENTAL PROCEDURES

Cloning of *cypX* from *Bacillus subtilis*. The gene encoding *cypX* from *B. subtilis* was amplified from a *B. subtilis* cell stab using oligonucleotides **sCypX_1**, GGGAGGAATTCAT-

GAGCCAATCGATTAAATTG (coding), and **sCypX_2**, CC-TTTGGACTCGAGTTATGCCCCGTCAAACGCAAC (non-coding), with concomitant incorporation of unique 5'-*EcoRI* and 3'-*XhoI* restriction sites. The *cypX* gene was subjected to a restriction digest using *EcoRI* and *XhoI*, purified by agarose gel electrophoresis, and cloned into the corresponding sites in the *E. coli* expression plasmid pET28a(+) (Novagen, Darmstadt, Germany) such that the expression of *cypX* was placed under the control of a T7 promoter. In this construct, the first codon of the CYP134A1 has a 14 amino acid N-terminal extension (MAS-MTGGGQMGRGSEF) before the last codon of the thrombin cleavage site of the pET28 construct. The resulting clone, pCypX1, was sequenced through the *cypX* reading frame to ensure that its sequence was that reported for wild-type *cypX*. A single mutation (G-1066 to A) was detected, conferring a mutation of Ala-356 to Thr-356 upon the CYP134A1 protein. Plasmid pCypX1 was then used to transform chemically competent BL21(DE3) *E. coli* cells.

QuikChange Repair of *cypX* A356T Clone. The gene encoding *cypX* A356T from above was converted to the originally reported sequence using a QuikChange kit (Stratagene) and employing oligonucleotides **sCypXRep_1**, CATAACTGTG-TAGGAGCAGCTTTCGCCAAGAACGAAATC, and **sCypXRep_2**, GATTTTCGTTCTTGGCGAAAGCTGCTCTACACAGTTATG, with the position of the repaired base underlined. Following the completion of the PCR reaction, parental template DNA was digested using *DpnI*, before the reaction was used to transform chemically competent DH5α *E. coli* cells. Clones were sequenced through the *cypX* reading frame to ensure that its sequence was that of wild-type *cypX*, with plasmid pCypX2 confirmed as containing the wild-type *cypX* gene. Plasmid pCypX2 was then used to transform chemically competent BL21(DE3) *E. coli* cells.

Protein Expression, Purification, and Characterization. (A) **General Procedures.** All purification steps were performed at 4 °C, with buffers filtered through a 0.2 μm filter and degassed prior to use. The protein concentration was determined using the method of Bradford using BSA as a reference protein (28). Cyclic dipeptides were purchased from Bachem (Bubendorf, Switzerland); other substrates were obtained from Sigma-Aldrich (Schnelldorf, Germany). All compounds used as substrates were of the highest purity available.

(B) **CYP134A1 Expression and Purification.** pCypX1 (for CYP134A1 A356T) or pCypX2 (for CYP134A1 wild type) transformed BL21(DE3) cells were grown overnight at 37 °C in TB + kanamycin (25 mg/L) to provide a starter culture for expression. Two × two liters of TB + kanamycin (25 mg/L) was then inoculated with 1% (v/v) of overnight culture and grown at 37 °C to an OD₆₀₀ of 0.5, whereupon the temperature was reduced to 18 °C and 0.5 mM δ-aminolevulinic acid was added. Expression of CYP134A1 was induced 20 min later using 0.1 mM IPTG. After 12 h at 18 °C, the cell pellet was collected by centrifugation at 4 °C (5000g), the pellet was resuspended in 50 mM Tris·HCl (pH 7.4), 50 mM NaCl, 1 mM PMSF, and 0.5 mM DTE, and the cells were lysed using two passes through a fluidizer (Microfluidics, Newton, MA). The lysis solution was clarified by centrifugation (120000g) and loaded onto a 5 mL Ni-NTA Superflow column (Qiagen, Hilden, Germany) that had been pre-equilibrated in 50 mM Tris·HCl (pH 8.0), 300 mM NaCl, and 20 mM imidazole. The column was washed with 5 column volumes of 50 mM Tris·HCl (pH 8.0), 300 mM NaCl, and 20 mM imidazole before the bound protein was eluted with

1.5 column volumes of 50 mM Tris·HCl (pH 8.0), 300 mM NaCl, and 250 mM imidazole. The eluted fractions were concentrated and buffer exchanged into 50 mM Tris·HCl (pH 8.0), 50 mM NaCl, and 0.5 mM EDTA using NAP-25 columns (GE Healthcare, Munich, Germany). The protein was purified using anion-exchange chromatography upon a ResourceQ column (GE Healthcare, Munich, Germany) attached to an Akta FPLC (GE Healthcare, Munich, Germany). Following loading, the column was washed with 3 column volumes of 50 mM Tris·HCl (pH 8.0), 50 mM NaCl, and 0.5 mM EDTA before the bound protein was eluted with a 6 column volume gradient with a final concentration of 60% 50 mM Tris·HCl (pH 8.0), 500 mM NaCl, and 0.5 mM EDTA. The eluted fractions were analyzed by SDS–PAGE and appropriate fractions pooled, concentrated, and purified by gel filtration on a Superose-12 column (GE Healthcare, Munich, Germany) attached to an Akta FPLC with a buffer condition of 50 mM Tris·HCl (pH 8.0) and 100 mM NaCl. The eluted fractions were analyzed by SDS–PAGE, appropriate fractions were pooled and concentrated using an Amicon Ultra centrifugal filter with a 30000 MW cutoff (Millipore, Bedford, MA), and aliquots were flash frozen in liquid nitrogen and stored at -80°C . The identity of the purified protein as CYP134A1 A356T or CYP134A1 wild type was confirmed by MALDI-TOF MS peptide map fingerprinting of tryptic digests of the excised SDS–PAGE protein bands. Selenomethionine-labeled CYP134A1 was expressed and purified using the same protocol as above with the following modifications: cells were grown in minimal media, supplemented with all amino acids except methionine, which was replaced with 50 mg/L selenomethionine. The induction phase of the preparation was extended to 24 h at 18°C .

(C) Binding of Cyclic Peptides and Related Compounds to CYP134A1. The binding of substrates to wild-type CYP134A1 was performed using UV–visible spectroscopy (V-630 spectrometer; JASCO, Gross-Umstadt, Germany) by monitoring the change in ligand environment of the heme iron due to water ligand displacement by substrate binding and thus a change from hexacoordinated iron(III) with an absorption maximum at 419 nm to pentacoordinated iron(III) with an absorption maximum at 392 nm for all substrates except 1-phenylimidazole and 4-phenylimidazole, where there is a change from hexacoordinated iron(III) with an absorption maximum at 419 nm to hexacoordinated, nitrogen atom coordinated iron(III) with an absorption maximum at 425 nm. CYP134A1 (2.0 μM) as a solution in 50 mM Tris·HCl (pH 7.4) and 100 mM NaCl was titrated with aliquots of the substrates in DMSO and the change in ligand environment heme iron monitored using the difference in absorbance between 419 and 392 nm (type 1 spectra) or 419 and 425 nm (type 2 spectra). Reactions were performed in triplicate for all substrates with the exception of the poor substrates cAA, cLG, and the sparingly soluble cLW. The binding of substrates was then using a one-site binding equation [bound ligand] = (capacity \times [free ligand]) / (K_d + [free ligand]) using the program GraFit 5. To determine the appropriateness for this equation under the wide range of binding constants observed, a quadratic binding equation was used for substrates cLL, cLF, cLP, and cLW: signal = initial signal + signal change \times ((([free ligand] + [protein] + K_d) / 2) - ((([free ligand] + [protein] + K_d) / 2)²) - ([ligand][protein])^{0.5}) / [protein]). The results indicate that the values provided by the simple hyperbolic equation and the quadratic equation are within experimental error for these substrates, which span the range of observed K_d values; therefore,

the simple equation was used to calculate the binding constants for substrates to CYP134A1 (K_d (μM): cLL 24.5 ± 0.5 (simple), 24.5 ± 0.5 (quadratic); cLF 11.5 ± 1.5 (simple), 10.4 ± 1.5 (quadratic); cLP 259 ± 49 (simple), 258 ± 50 (quadratic); cLW 2.6 ± 1.3 (simple), 1.6 ± 2.1 (quadratic)). The percentage spin state change for type 1 ligand binding was calculated using the extinction coefficient values reported for P450_{cam} (29, 30) and P450_{terp} (31). The binding of imidazole and cLL to the A356T CYP134A1 protein was also tested and found to be the same as for the wild-type protein (results not shown).

(D) Turnover Experiments. Triplicate turnovers of cLL (100 μM) were performed in 20 mM Tris·HCl (pH 7.4, room temperature) and 50 mM NaCl at 37°C for 60 min with shaking using wild-type CYP134A1 (0.5 μM), reductase (0.5 μM), ferredoxin (5.0 μM), and NAD(P)H (1 mM) with a final volume of 1 mL. Electron transfer partners used were palustrisredoxin reductase (PuR)/palustrisredoxin (Pux)/NADH; PuR/palustrisredoxin B (PuxB) (*Rhodospseudomonas palustris* CGA009 (32)) / NADH; *Novosphingobium aromaticivorans* ArR reductase/Arx ferredoxin/NADH (33); *R. palustris* HaA2 HaPuR reductase/HaPux ferredoxin/NADH (34); and spinach ferredoxin reductase/spinach ferredoxin/NADPH. All redox partners were purified as previously reported (33, 34), with the exception of spinach ferredoxin reductase and spinach ferredoxin, which were purchased from Sigma-Aldrich. Controls were performed exactly as turnover experiments with the omission of either NAD(P)H or CYP134A1. Triplicate turnovers of cLF and cMM were performed as described above, using the selected redox systems only (cLF, PuR/Pux/NADH, ArR/Arx/NADH, HaPuR/HaPux/NADH; cMM, PuR/Pux/NADH).

Triplicate turnovers of cLL (100 μM) making use of the peroxide shunt pathway were performed in 20 mM Tris·HCl (pH 7.4, RT) and 50 mM NaCl at 37°C for 30 min with shaking using wild-type CYP134A1 (0.5 μM) and hydrogen peroxide (~ 10 mM), *m*-chloroperbenzoic acid (1 mM), or trifluoroperacetic acid (1 mM) with a final volume of 1 mL. Peroxide oxidants were added in a total of 10 aliquots, once every 3 min to afford the final peroxide concentration noted above. Controls were performed exactly as turnover experiments with the omission of either peroxide or CYP134A1.

Following completion of the reactions, the turnover samples were acidified with TFA (20 μL) before being loaded onto Strata-X reversed-phase SPE cartridges (30 mg/mL; Phenomenex, Aschaffenburg, Germany) that had been activated with methanol (300 μL) and equilibrated with 0.1% aqueous TFA (600 μL). The cartridges were subsequently washed with 0.1% aqueous TFA (600 μL) before being dried under vacuum for 15 min. The dried cartridges were then eluted using ethyl acetate (300 μL). The eluent was divided into separate vials before being treated with either trimethylsulfonium hydroxide (0.2 M in methanol), *N*-(trimethylsilyl)imidazole, or *N*-methylbis(trifluoroacetamide) (Macherey-Nagel, Düren, Germany).

The reactions were allowed to proceed for 15 min before being analyzed by GCMS (Shimadzu GCMS-QP-2010 Plus; Shimadzu, Darmstadt, Germany) using an Rxi-5 ms column (30 m, 0.25 mm internal diameter; Restek, Bad Homburg, Germany). GC Program for analysis of the turnovers by CYP134A1 on a Rxi-5 ms column: split mode; column flow 2.5 mL/min; split ratio 5; total flow 17.9 mL/min; injector 250°C ; detector 250°C ; oven 100°C (1.0 min equilibration) hold for 2.0 min, ramp $5^{\circ}\text{C}/\text{min}$ to 250°C and hold for 10.0 min (total program time 42.0 min).

Identification of compounds was performed using mass spectral fragmentation analysis; see SI Table 1.

(E) Protein Crystallization, Data Collection, and Structure Determination. Crystals were grown by hanging drop vapor diffusion. The CYP134A1 A356T protein (7 mg/mL) was mixed 1:1 with the reservoir solution (0.1 M Bis-Tris (pH 6.5), 0.1 M MgCl₂, 12% (w/v) polyethylene glycol 3350) and equilibrated against the reservoir solution. After 2–4 days thin red plates had formed. The crystals were passed through a cryoprotectant solution containing 0.1 M Bis-Tris (pH 6.5), 0.1 M MgCl₂, 12% (w/v) polyethylene glycol 3350, and 25% (v/v) glycerol before flash cooling in liquid nitrogen.

Compound soaks were performed either by inclusion of the compound of interest in the cryoprotectant solution or by addition to the crystals in the crystallization drop. For inclusion in the cryoprotectant the following concentrations were used: cyclic dipeptides cLL and cMM 1 mM (50 mM stock solution in DMSO); cyclic dipeptide cAA 10 mM (100 mM stock solution in water); imidazole 50 mM (500 mM stock solution in water); phenylimidazole compounds 10 mM (100 mM stock solution in DMSO). The crystals were allowed to equilibrate for 2–10 min. For the addition of the compound directly to crystals in the drop, the following concentrations were used: cyclic dipeptides cLL and cMM 1.5 mM (50 mM stock solution in DMSO); cyclic dipeptide cAA 10 mM (100 mM stock solution in water).

Cocrystallization of cLL with CYP134A1 was performed with both the wild-type and A356T mutant protein under the same conditions as indicated above but with the addition of 1.5 mM cLL (50 mM stock solution in DMSO) to the protein prior to drop setup and incubation for 15 min at room temperature.

Diffraction data were collected at beamline X10SA at the Swiss Light Source, with the crystal kept at 100 K and processed using the XDS program suite (35). All crystals are in space group *P*2(1)2(1)2(1) with two CYP134A1 molecules per asymmetric unit. Protein crystals grown from selenomethionine-labeled A356T CYP134A1 were used for phasing by seleno single anomalous diffraction (3.1 Å resolution). Twenty-five selenium positions were identified by SHARP (36), and after density modification, interpretable electron density maps were obtained. Automatic rebuilding was not successful, instead the heme density was identified manually and then used to orient truncated structures of P450_{Biol} (Protein Data Bank code 3EJB, chain B) and EryF (Protein Data Bank code 1EGY, chain A) as guide structures that were then appropriately altered and extended manually in COOT (37) following a simulated annealing procedure in CNS (38). During several cyclic rounds of refinement with REFMAC (39) and manual rebuilding, heme and solvent molecules were included in the model. The native crystal structures were built using the selenomethionine structure as an initial model manually in COOT, with cyclic rounds of refinement with REFMAC employing TLS refinement (40), during which heme, solvent molecules, and ligands (where appropriate) were included in the model. TLS input files were generated using the TLS-Motion Determination Server (41, 42). Structure validation was performed using MOLPROBITY (43) and PROCHECK (44). Structure-based sequence alignments were carried out with SSM (45) as implemented in COOT, with secondary structure analysis of the final structure performed using the DSSPcont server (46) and comparisons to known structures performed using DaliLite (47). All structural figures were prepared using PyMol (48). Electrostatic properties were calculated using the program APBS (49) as implemented in PyMol (48). Docking was

performed using program the AUTODOCK (50) and the PatchDock server (51).

(F) Sequence Alignments. Sequence alignments were performed using the ClustalW2 server at EMBL-EBI (52). Similar sequences were determined using BLAST (53) as implemented by the ExPASy Proteomics Server (54).

RESULTS

CYP134A1 Protein Expression. CYP134A1 was cloned from the genomic DNA of *B. subtilis* strain 168, which initially afforded a gene that differed from the deposited sequence by a single base mutation (leading to a Ala-356 to Thr-356 mutation). A blast search and alignment of the best matches indicated that the mutation was likely to be a cloning artifact, and thus the clone was repaired to the expected wild-type sequence. Recombinant CYP134A1 expresses well in *E. coli*, with cells distinctly red following induction. The wild-type and mutant enzymes were purified in a three-step process utilizing an initial Ni-NTA affinity step, followed by anion-exchange chromatography and a final gel filtration step to afford pure protein (>95% as visualized by SDS–PAGE) with a ratio of 419 nm to 280 nm absorbance (1.5) that agrees well with the values reported for other prokaryotic P450s (29–31).

UV Characterization and Substrate Binding. UV–visible spectroscopy of the purified CYP134A1 wild-type and A356T mutant protein gives a typical substrate-free P450 absorption spectrum, with λ_{max} at 419 nm and the α - and β -bands at 570 and 538 nm, respectively. Titration of CYP134A1 with imidazole yields a standard type 2 spectrum with the λ_{max} shifting to 425 nm, indicative of nitrogen coordination to the heme iron. Titration of CYP134A1 with cLL showed a shift in λ_{max} from 419 to 392 nm, indicating a binding interaction with an average dissociation constant of $24.5 \pm 0.5 \mu\text{M}$ and with a large change in spin state of the iron (Table 1). The binding of cLL to the A356T mutant protein affords the same average dissociation constant as for the wild-type protein (data not shown). The effect of the cyclic dipeptide side chains on substrate binding to CYP134A1 was explored with a range of cyclic peptides (cAA, cVV, cLG, cLP, cLF, cLW, cMM, Table 1). In general, substrates with small alkyl groups (cAA, cLG, cLP) exhibit weaker binding to CYP134A1 and do not promote a high degree of spin state change of the heme iron. Substrates with larger hydrophobic side chains bind in a similar regime to cLL (including cMM and cLF; cLW exhibits severe solubility problems in aqueous solution making data for this ligand unreliable), while the substrate cVV falls in the middle in terms of both binding constant and spin state change. 2,5-Dimethylpyrazine and 2,3,4,5-tetramethylpyrazine do not exhibit any effect on the heme iron environment of CYP134A1, while di-*tert*-butylhydroxyquinone and di-*tert*-butylquinone bind to CYP134A1 (Table 1). Binding of the quinone compound is slightly stronger than the hydroxyquinone compound, although the degree of spin state change in the case of the quinone form is significantly higher. 1-, 2-, and 4-phenylimidazoles also bind to CYP134A1, although with widely varying affinities (Table 1).

Crystallization and Structure Determination. CYP134A1 A356T crystallizes under several PEG-3350 conditions, with an optimum pH around 6 and a relatively low PEG concentration (12–15% (w/v)). Curiously, the wild-type protein does not crystallize under these conditions, while the protein of the A356T mutant crystallizes readily and forms large, thin plates. The structure of CYP134A1 was determined using single anomalous dispersion measurements of crystals grown from

Table 1: Substrate Binding Affinities and Changes in Soret Absorption of CYP134A1 for a Range of Cyclic Dipeptides and Substrate Analogues

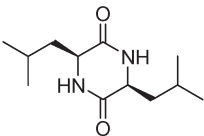
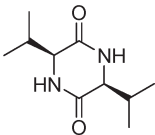
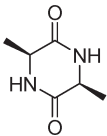
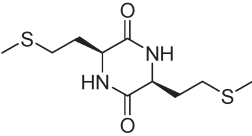
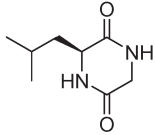
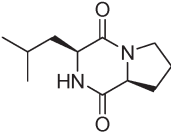
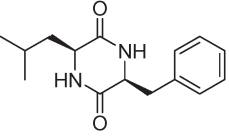
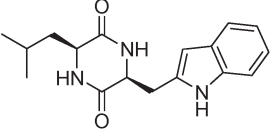
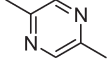
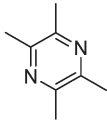
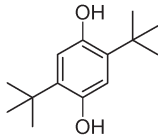
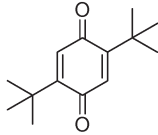
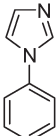
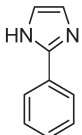
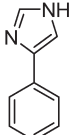
Substrate	K_d (μM)	Soret maximum (bound)	Maximal $\Delta(\text{Abs}_{\text{bound}} - \text{Abs}_{\text{unbound}})^b$	Relative $\Delta(\text{Abs}_{\text{bound}} - \text{Abs}_{\text{unbound}})^c$
 Cyclo(-Leu-Leu) cLL	24.5 ± 0.5	392 nm	0.210 ± 0.004	100 ± 2
 Cyclo(-Val-Val) cVV	137 ± 10	392 nm	0.098 ± 0.010	47 ± 5
 Cyclo(-Ala-Ala) cAA	1684 ± 13	392 nm	0.210 ± 0.004	3 ± 2
 Cyclo(-Met-Met) cMM	113 ± 11	392 nm	0.186 ± 0.006	89 ± 3
 Cyclo(-Leu-Gly) cLG	321 ± 13	392 nm	0.012 ± 0.006	6 ± 3
 Cyclo(-Leu-Pro) cLP	259 ± 49	392 nm	0.054 ± 0.014	26 ± 7
 Cyclo(-Leu-Phe) cLF	11.5 ± 1.5	392 nm	0.208 ± 0.002	99 ± 1
 Cyclo(-Leu-Trp) cLW	2.6 ± 1.3	392 nm	0.032 ± 0.010	15 ± 5
 Dimethylpyrazine	No Binding	N/A	No Shift	0
 Tetramethylpyrazine	No Binding	N/A	No Shift	0

Table 1. Continued

Substrate		K_d (μM)	Soret maximum (bound)	Maximal $\Delta(\text{Abs}_{\text{bound}} - \text{Abs}_{\text{unbound}})^b$	Relative $\Delta(\text{Abs}_{\text{bound}} - \text{Abs}_{\text{unbound}})^c$
	2,5-di- <i>t</i> -butylhydroxyquinone	117 ± 17	392 nm	0.055 ± 0.002	26 ± 1
	2,5-di- <i>t</i> -butylquinone	76.5 ± 11.5	392 nm	0.174 ± 0.004	83 ± 2
	1-phenylimidazole	57.0 ± 23.5	425 nm (Type 2 spectrum) ^a	0.088 ± 0.012	52 ± 7
	2-phenylimidazole	230 ± 59	392 nm	0.092 ± 0.002	44 ± 1
	4-phenylimidazole	11.3 ± 3.9	425 nm (Type 2 spectrum) ^a	0.095 ± 0.007	56 ± 4

^aType 2 spectra are indicative of a nitrogen atom coordinating to the heme iron. ^bAbsorption Soret maximum (bound) shown in the fourth column; absorption Soret maximum (unbound) 419 nm. ^cRelative $\Delta(\text{Abs}_{\text{bound}} - \text{Abs}_{\text{unbound}})$ shown as a percentage of the largest $\Delta(\text{Abs}_{\text{bound}} - \text{Abs}_{\text{unbound}})$ for type 1 spectra (shift to 392 nm, cLL and cLF) or type 2 spectra (shift to 425 nm, imidazole).

selenomethionine-labeled CYP134A1 A356T (Table 2). Model building was performed manually following the failure of automated routines (Table 2).

The structure of CYP134A1 adopts the canonical P450 fold, with primarily α -helical structure surrounding a noncovalently linked iron protoporphyrin IX (heme) moiety (Figure 2A). There is no electron density for portions of the B–B₂ loop in CYP134A1 and the N-terminal portion of the C-helix, indicating significant disorder in these regions. The B–B₂ loop also exists in two different forms in the crystal structures obtained: a more looplike “open” conformation giving rise to a larger active site (present in the native-1 structure, monomer A, and both monomers in the native-2 structure) and a “closed” conformation in which the B₂ helix is formed and the active site is more compact (present in monomer B in the structure of native-1) (Figure 2B). The arrangement of the loop in the B-monomer appears to be dependent on the age of the crystal, with older crystals (> 3 days after crystal formation) adopting the open conformation. The mutated Thr-356 residue interacts via hydrogen bonds from its side chain hydroxyl group with the backbone carbonyl oxygen of

Cys-353 (2.7 Å) and the side chain nitrogen of Asn-352 (3.2–3.6 Å), possible causes for the crystallization of the A356T mutant but not the wild-type protein.

The two CYP134A1 monomers (A and B) in the asymmetric unit of the crystal lattice are highly similar in structure, excluding alterations in the B–B₂ loop noted above (native-1 structure, root-mean-square deviation (rmsd), C α) 0.6 Å; native-2 structure, rmsd (C α) 0.5 Å). Comparison of both monomers in the asymmetric unit of native-1 to native-2 also affords an rmsd (C α) of 0.6 Å, with the same rmsd also seen for comparison of the phenylimidazole-bound structures to that of native-1.

Comparison of the CYP134A1 structure to other P450 structures in the Protein Data Bank (PDB) (see SI Table 3 for details) gives the best match to CalO2 (rmsd 2.2 Å, PDB code 3BUJ), a P450 believed to be a orsellenic acid oxidase from the calicheamicin biosynthetic operon of *Micromonospora echinospora* (55). CYP134A1 also matches well to P450_{BioI}, a fatty acyl-ACP oxidase found in the biotin operon of *B. subtilis* (rmsd (C α) 2.0 Å, PDB code 3EJB) (56). Curiously, both are either believed (CalO2) or are known (P450_{BioI}) to act upon carrier

Table 2: Crystallographic Data for A356T CYP134A1 Structures

data collection	CYP134A1 SelMet	CYP134A1 native 1	CYP134A1 native 2	1-Phe imidazole	2-Phe imidazole
space group	<i>P</i> 2 ₁ 2 ₁ 2 ₁	<i>P</i> 2 ₁ 2 ₁ 2 ₁	<i>P</i> 2 ₁ 2 ₁ 2 ₁	<i>P</i> 2 ₁ 2 ₁ 2 ₁	<i>P</i> 2 ₁ 2 ₁ 2 ₁
cell dimensions <i>a</i> , <i>b</i> , <i>c</i> (Å)	63.8, 104.3, 142.9	63.8, 105.4, 143.9	63.8, 105.4, 143.9	65.0, 106.9, 142.3	64.4, 106.8, 142.1
molecules in asymmetric unit	2	2	2	2	2
X-ray source	SLS X10SA	SLS X10SA	SLS X10SA	SLS X10SA	SLS X10SA
wavelength (Å)	0.9794	0.9790	1.0000	0.9790	0.9790
resolution (Å) ^a	50.0–3.10 (3.18–3.10)	50.0–2.66 (2.73–2.66)	50.0–2.90 (2.98–2.90)	50.0–3.10 (3.18–3.10)	50.0–3.30 (3.39–3.30)
<i>R</i> _{sym} ^a	0.09 (0.33)	0.14 (0.58)	0.11 (0.36)	0.11 (0.43)	0.12 (0.39)
<i>I</i> / <i>σ</i> ^a	16.4 (5.1)	8.3 (2.1)	8.4 (3.8)	12.9 (4.0)	14.4 (5.1)
completeness (%) ^a	96.0 (87.4)	91.3 (80.8)	96.4 (90.7)	94.3 (86.6)	95.8 (89.4)
redundancy	7.8	3.8	3.9	4.8	4.8
Wilson <i>B</i> -factor (Å ²)	60.3	62.9	68.5	72.8	55.9
phasing	FOM (25 sites) 0.38 phasing power (anomalous) 1.41	N/A	N/A	N/A	N/A
refinement	N/A	26005	21266	17646	14694
unique reflections	32093	47.7–2.66	40.6–2.90	48.1–3.10	47.7–3.30
resolution in refinement		0.219/0.273	0.231/0.306	0.214/0.278	0.211/0.289
<i>R</i> _{work} / <i>R</i> _{free} ^b		A and B; C and D	A and B; C and D	A and B; C and D	A and B; C and D
NCS groups (chain)		A6–104, A105–167, A168–291, A292–403; B6–104, B105–167, B168–330, B331–404	A6–10, A11–109, A110–154, A155–290, A291–403; B6–10, B11–116, B117–186, B187–336, B337–403	A5–102, A103–150, A151–290, A291–353; A354–403; B4–66, B67–104, B105–168, B169–290, B291–404	A5–57, A58–107, A108–200, A201–296, A297–403; B6–101, B102–167, B168–290, B291–391, B392–404
TLS groups					
no. of atoms		6060	6005	6036	6027
protein		(A5–73, A87–210, A217–403; B5–75, B86–211, B217–404)	(A6–73, A86–213, A216–403; B6–68, B90–212, B217–403)	(A5–68, A87–210, A218–403; B4–73, B86–404)	(A5–71, A87–211, A217–403; B6–74, B86–212, B217–404)
heme		86	86	86	86
ligand		0	0	22	22
glycerol		12	12	0	0
water		46	32	5	2
Mg ions		6	3	1	2
<i>B</i> -factors ^c					
protein		56.8	58.9	63.2	48.5
heme		27.7	20.0	23.6	15.4
ligand		N/A	N/A	54.0	62.3
glycerol		56.1	40.1	N/A	N/A
water		45.9	55.9	47.0	42.5
Mg ions		42.1	46.3	73.0	28.5
rmsd					
bond lengths (Å)		0.011	0.009	0.012	0.010
bond angles (deg)		1.327	1.254	1.490	1.253
Ramachandran statistics ^d					
residues favored (%)		95.2	95.8	93.9	94.4
disallowed residues		0	0	2	1
unusual rotamers (%)		0.9	0.8	1.4	1.1
PDB code		3NC3	3NC5	3NC6	3NC7

^aNumbers in parentheses correspond to the values from the highest resolution shell. ^b $R_{\text{work}} = \sum |F_o| - |F_c| / \sum |F_o|$, calculated from the working reflection set; R_{free} calculated in the same manner using the 4–5% test reflection set. ^c*B*-factors for protein residues determined using TLSANL; heme, glycerol, ligand, and water *B*-factors not corrected. ^dCalculated by MOLPROBITY (43); percentage of the protein residues in most favored regions; disallowed residues and percentage of unusual rotamers.

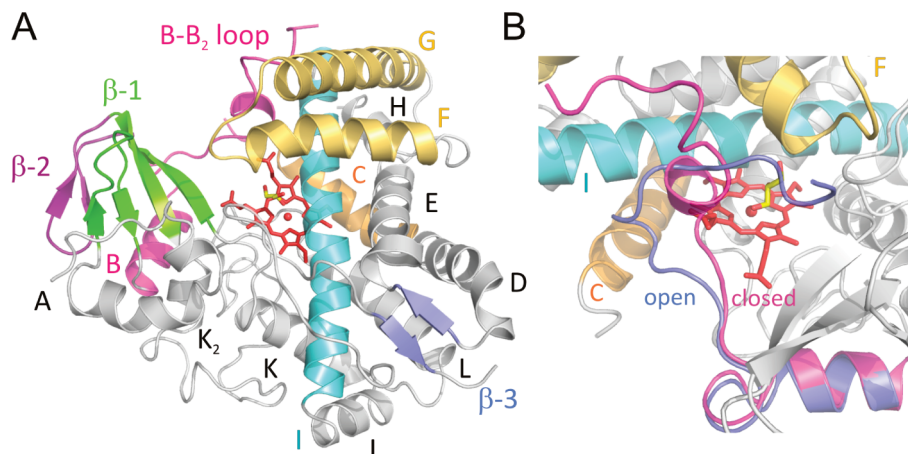


FIGURE 2: (A) Overall structure of CYP134A1 (glycerol molecules shown in yellow, majority of CYP134A1 shown in gray with certain structural motifs colored for clarity; the heme is shown in red) with structural motifs labeled. (B) Alternate conformations of the B–B₂ loop (majority of CYP134A1 shown in gray with the B–B₂ loop colored in pink in the closed form and in blue in the open form; the heme is shown in red) with selected structural motifs labeled.

protein-bound substrates, which is not the case with CYP134A1. Other structurally similar P450s to CYP134A1 are involved in macrolide functionalization, such as the hydroxylases EryF (rmsd (C α) 2.2 Å, PDB code 1OXA) (57) and EryK (rmsd (C α) 2.3 Å, PDB code 2WIO) (58), isolated from the erythromycin operon of *Saccharopolyspora erythraea* and PikC (rmsd 2.1 Å, PDB code 1Q5E), involved in epothilone epoxidation in *Sorangium cellulosum* (59).

Active Site Architecture. The active site of CYP134A1 is formed by several structural elements that are composed mainly of hydrophobic residues. One crucial structural element is the N-terminal and central regions of the I-helix (residues 229–237), which runs across the face of the heme and occludes somewhat more of the heme surface than what is seen in the closest matching P450 structures (Figure 3). The opposite side of the active site to the I-helix is formed by portion of the β -1 sheet and residues immediately preceding the sheet (residues 278–285, Figure 3). This region adopts the same position as that observed in the closest matching structures despite of the presence of three proline residues in this eight amino acid sequence. The C-terminal end of the F-helix forms the majority of the ceiling above the active site (residues 158–166, Figure 3). Residues Tyr-391 and Thr-392, present in the long C-terminal loop of CYP134A1, also contribute to forming the active site ceiling. Tyr-391 exists in different conformations in the different structures, exhibiting side chain orientations that either point into or out of the active site of CYP134A1 in the substrate-free form, or a position halfway in between the substrate free orientations when a phenylimidazole ligand is bound. The position of the tyrosine side chain depends upon the presence of a glycerol molecule in the active site, due to the presence of a hydrogen bond between the phenol group and a glycerol oxygen atom (Figure 3). The most solvent exposed portion of the active site corresponds to the B–B₂ loop region, which adopts several conformations in the CYP134A1 structures discussed here, neither of which follows the typical conformation seen in other P450s. The two major conformations are an “open” configuration, with the B–B₂ loop running essentially parallel to the G-helix and not impinging upon the active site, or a “closed” conformation, where a short B₂ helix forms perpendicular to the heme and residues Leu-64 and Arg-67 project into the active site cavity (residues 61–73/75 are visible in the “open” and “closed” forms, respectively). The “closed” form is also observed in the

phenylimidazole-bound structures, and it is likely that the B–B₂ loop rearranges upon substrate binding. The “closed” conformation of the CYP134A1 B–B₂ loop is too small to accommodate cLL, suggesting that this structure represents a collapsed active site formed in solution in the absence of substrate.

The active site of CYP134A1 does not contain the conserved catalytic residues typically observed in P450s, specifically the highly conserved acid/alcohol residue pair (CYP134A1 residues 236–237) that controls protonation of intermediate oxygen species during oxygen activation (4). In CYP134A1 the alcohol residue is replaced by a proline, Pro-237, which cannot be involved in hydrogen-bonding interactions with solvent to control the activation of oxygen. Examples of the acid/alcohol pair not being conserved are found with P450s where substrate hydroxyl groups assist in the formation of the appropriate hydrogen-bonding arrangement to allow correct oxygen protonation (EryF and EryK) (55, 59), in situations where the P450 functions as a per-oxygenase (Bs β) (60, 61), or where the P450 catalyzes an unusual reductive denitration (XplA degradation of RDX) (62). The proximal heme thiolate ligand Cys-353 is present in the N-terminal loop prior to the L-helix, while coordination of the heme propionate groups achieved through the interaction of one propionate with the guanidinium moiety of Arg-285 (2.7 and 2.8 Å in the native-1 structure), with additional hydrogen bonding in the B-monomer provided by His-351 (3.1 Å). The other heme propionate group is essentially without hydrogen-bonding partners except in the case of the A-monomer where a weak hydrogen bond of 3.2 Å to Lys-62 is formed. Residues of the C-helix, B–B₂ loop, and the loop prior to the L-helix that might be expected to interact with this propionate group are not correctly positioned in any structure to do so; the conformation observed within the crystal for these elements is only influenced by crystal contacts in the case of the “closed” conformation of the B–B₂ loop, where Arg-73 interacts with residues in the D-helix of a neighboring monomer. The lack of heme binding residues in the CYP134A1 crystal structures indicates that an alternate conformation of the B–B₂ loop region upon substrate binding is probable. The “closed” conformation may also play a role in solution in excluding water from the active site in the absence of substrate, where the positioning of the heme residue is not as critical. In the substrate-free structures there is a water molecule bound to the heme iron at a distance of 2.0 Å, and at least one

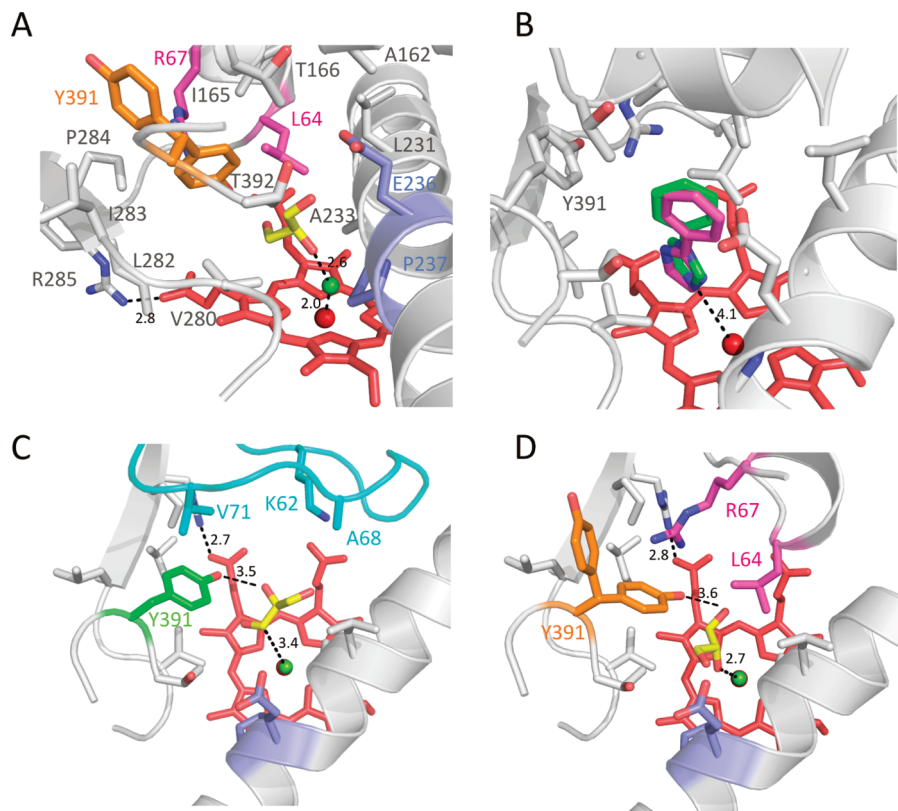


FIGURE 3: Active site of CYP134A1. (A) Closed conformation of the B–B₂ loop, indicating the largely hydrophobic nature of the active site (B–B₂ loop residues involved in forming the active site pocket shown in magenta, the two conformations of Tyr-391 shown in orange). (B) Phenylimidazole ligand bound structures (1-phenylimidazole shown as green sticks, 2-phenylimidazole shown as pink sticks). (C, D) Effects of the alternate B–B₂ loop conformations upon the active site pocket (open B–B₂ loop and residues forming the active site shown in turquoise, closed B–B₂ loop residues forming the active site shown in magenta, Tyr-391 conformations shown in green for the open B–B₂ loop and in orange for the closed B–B₂ loop); for all, hydrogen-bonding distances indicated by dashed lines, glycerol shown as yellow sticks, water shown as a green sphere, heme shown in red, catalytically important residues shown in blue, majority of CYP134A1 shown in gray.

glycerol molecule is also present in the active site of CYP134A1. The glycerol molecules located in the cavity above the heme are in different conformations in the two different monomers of the asymmetric unit. Despite this, the closest atoms to the heme are in a similar position as the imidazole ring in the phenylimidazole-bound structures.

Ligand-bound structures were obtained for CYP134A1 by soaking crystals with either 1-phenylimidazole or 2-phenylimidazole. Both compounds adopt the same orientation, with the imidazole moiety closest to the heme iron and the imidazole and phenyl rings perpendicular to the plane of the heme. The heme iron to the ligand nitrogen atom distance is 4.1 Å for the 1-phenylimidazole structure, longer than that seen in iron–nitrogen ligation of other such ligands to heme iron containing proteins (2.1–2.4 Å; PDB codes 1F4T, 1PHF, 2Q6N, and 1EGX), although photoreduction of the iron may explain some of this apparent increase in distance. The 2-phenylimidazole-soaked structures afford the same average heme iron to nearest ligand atom distance, with the ligand occupying essentially the same orientation. In both soaked structures, the B-monomer with the B–B₂ loop in the closed conformation affords better defined density for the ligand, while in the A-monomer, the presence of the 1-phenylimidazole ligand causes the B–B₂ loop to rearrange into the closed conformation. The density observed for the 2-phenylimidazole ligand in the A-monomer is poorer than in the case of 1-phenylimidazole, and the loop is still predominantly in the open conformation, although there is density present for the closed conformation. The effect of ligand binding upon active site

residue Tyr-391 is marked, with the amino acid side chain sensing the presence of ligand and adopting a single conformation, with the phenyl ring projecting out of the active site.

One region that distinguishes CYP134A1 from the majority of P450s is the presence of a ten-residue helix–loop insertion (residues 332–341) prior to the heme ligating cysteine ligand on the proximal side of the heme. This inserted sequence occurs at a region of the P450 where normally redox partner proteins interact with the P450, delivering electrons to allow the normal P450 cycle to occur. The presence of this insertion sequence is yet another curious divergence from typical bacterial P450 structure along with the proline present in the active site.

Sequence Comparison of CYP134A1 with Closely Related P450s. A BLAST search and sequence analysis of the closest sequence matches to CYP134A1 from *B. subtilis* indicates that the closest matches can be divided essentially into three groups on the basis of conservation of sequence motifs (see SI for a full discussion). The group that contains CYP134A1 from *B. subtilis* includes ten P450s often annotated as “CypX” that possess sequences with a very high degree of sequence conservation in the P450 substrate recognition sites (SRSs) (SI Table 4); it would appear that these enzymes catalyze a similar reaction as in the case of CYP134A1 in these organisms.

Comparison of CYP134A1 to Related P450 Structures. Excluding the highly variable B–B₂ loop region, the structures of CYP134A1 and the structures of P450_{Biol} (56, 63–65) and CalO2 (55) possess very similar active site geometries around the heme. The more restricted active site of CYP134A1 is

Table 3: Oxidation of Cyclic Dipeptides by CYP134A1

substrate	redox system	total product formation (%) ^a	relative production ^b
cLL	SpFd/SpFdR/NADPH	1.2 ± 1.0 ^c	1.0
cLL	Pux/PuR/NADH	1.1 ± 0.3 ^c	0.9
cLL	HaPux/HaPuR/NADH	0.7 ± 0.4 ^c	0.6
cLL	Arx/ArR/NADH	0.5 ± 0.1 ^c	0.4
cLL	PuxB/PuR/NADH	0.1 ± 0.1 ^c	0.1
cLF	Arx/ArR/NADH	0.4 ± 0.3 ^c	0.3
cLF	Pux/PuR/NADH	0.3 ± 0.1 ^c	0.3
cLF	HaPux/HaPuR/NADH	0.2 ± 0.1 ^c	0.1
cMM	Pux/PuR/NADH	4.3 ± 0.8 ^d	3.7

^aProduct formation calculated based upon the ratio of residual substrate to product; uncorrected for individual MS response due to lack of authentic standards. ^bRelative production of product compared to the most efficient redox system sustaining cLL oxidation. ^cMonooxygenated product. ^dAromatized product.

engineered through a shorter B–B₂ loop region, which also appears to be the substrate entry channel for CYP134A1. The catalytically important alcohol active site residue is present in all structures closely related to CYP134A1 (which has a proline in this position), with the one exception being the erythromycin hydroxylase EryF (57), where this residue is replaced with an alanine residue. Correct protonation of oxygen in the case of EryF is ensured by the interaction of a substrate hydroxyl group in the hydrogen-bonded water network making up the EryF active site (57, 66). The 332–341 residue loop extension in CYP134A1 is not present in any comparable structure: this longer loop possibly impedes the access of solvent to the proximal heme face and the binding of electron transfer proteins.

CYP121 catalyzes the phenolic coupling of the two tyrosine phenolic rings in cYY through a diaryl bridge (67). The structure of cYY bound to CYP121 indicates that the phenolic oxygen of cYY is a relatively long distance away from the heme iron (6.5 Å), with a water molecule still bound to the heme iron even in the presence of the cYY substrate. CYP121 makes few hydrogen-bonding interactions with cYY, with only one direct hydrogen bond to cYY and four mediated through water molecules. The difference in the oxidation reactions catalyzed by CYP134A1 and CYP121 requires the cYY phenol side chains to be presented close to the heme iron of CYP121 and not the diketopiperazine ring: the reverse is true for CYP134A1. Unsurprisingly, this needs different active site constraints, with CYP121 containing a large number of aromatic residues and a more polar active site than that of CYP134A1. CYP121 makes use of a typical P450 oxidative cycle, possessing the conserved active site alcohol residue and lacking the proximal heme loop extension seen in CYP134A1.

Substrate Turnover Experiments. Attempted oxidation of the cLL substrate by CYP134A1 wild-type protein was performed at 37 °C using five different pairs of redox partner proteins and a 10-fold excess of NAD(P)H. Analysis of the results of turnover using GCMS following SPE extraction and derivatization of the samples with TMSH (see SI Table 1) indicated low levels of product formation (Table 3) varying among the different reactions, with the highest level of product formation occurring in the turnovers where the redox systems were palustrisredoxin reductase and the palustrisredoxin ferredoxin from *R. palustris* (32) (see SI Figure 2) and spinach ferredoxin reductase and ferredoxin (Table 3). Analysis of the retention time and MS of the product indicated that it is likely to be a methylated phenol tautomer of cLL with the incorporation of one oxygen atom (SI Table 1, Figure 4). To determine whether

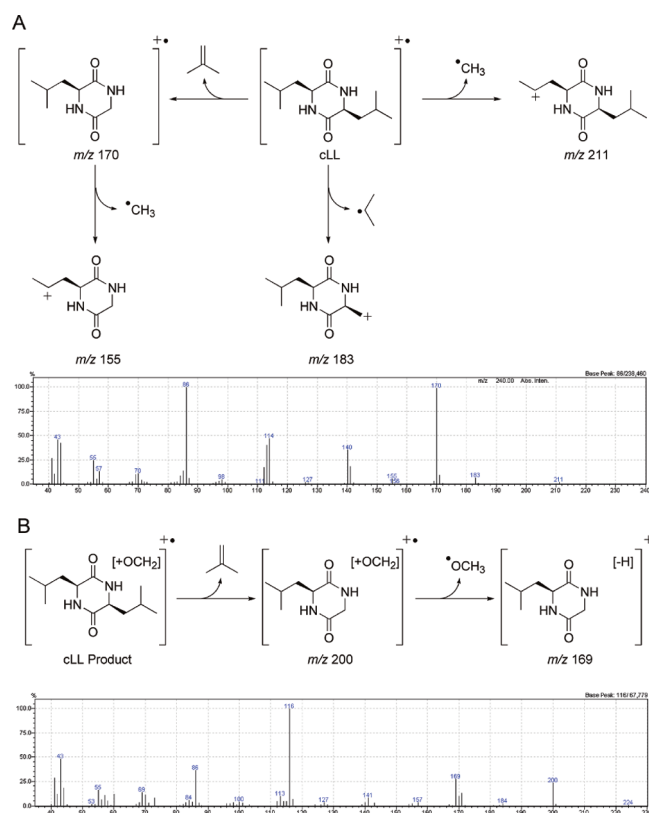


FIGURE 4: MS fragmentation of cLL (A) and the oxidized cLL product (B), showing the mass spectra and the postulated fragmentation pathways for notable ions.

peroxide could act as an oxidant in conjunction with CYP134A1, turnovers of cLL were attempted in the presence of hydrogen peroxide, *m*-chloroperbenzoic acid, and trifluoroperacetic acid. None of these reactions afforded any products as identified by GCMS. Turnover of cLF using selected redox partners indicated a low level of comparable product (SI Table 1, SI Figures 2 and 3). Turnover of cMM did not give a comparable product to cLL and cLF; rather there was the appearance of an aromatized product with both phenol oxygens derivatized as the methyl ethers (SI Table 1, SI Figures 2 and 4). The products formed indicate that the oxidation of the cLL/cLF ligands occurs via the same hydroxylation mechanism, with the mechanism of oxidation of cMM either the same with concomitant dehydration or occurring through an alternate electron transfer process.

Docking Studies. Docking of cLL to the two different active site configurations observed in the CYP134A1 crystal structures

using Autodock (50) and Patchdock (51) indicate that binding of cLL to CYP134A1 is only feasible in the open form of the active site, with the closed form being too restricted to accept the cLL substrate. In the open form of the active site, the best docking solutions were obtained where one diketopiperazine ring nitrogen is 6.2–6.6 Å from the heme iron (SI Figures 5 and 6). In these cases, the distance from the closest diketopiperazine methine carbons to the heme iron is in the range of 7.6–8.2 Å. The docked models of cLL generated by Autodock (where amino acid side chains are mobile) indicate a hydrogen-bonding interaction between Tyr-391 and one of the cLL diketopiperazine ring nitrogen atoms, in a manner similar to that seen for the bound glycerol molecules in the *apo* CYP134A1 structures. The inability for the closed conformation to accommodate the cLL substrate indicates that this is not a mimic of the substrate-bound state; rather this closed conformation is likely to stem from hydrophobic interactions between the B–B₂ loop and the active site, thus excluding water from the active site.

DISCUSSION

Substrate Binding Studies and Substrate Selectivity. The substrate requirements for binding to CYP134A1 were explored using a number of different cyclic dipeptides and substrate analogues. Screening eight cyclic dipeptides against CYP134A1 showed that cLL, formed by the preceding YvmC protein (13), binds with an affinity of $24.5 \pm 0.5 \mu\text{M}$ and that the protein exhibits a high degree of change in spin state from low to high spin indicating complete displacement of the resting state heme iron water ligand. Comparing this binding constant to that seen for the binding of cYY to CYP121 ($21.3 \pm 3.5 \mu\text{M}$), the only other cyclic dipeptide binding P450 characterized to date, indicates that the binding constants for these two P450s are very similar.

The smaller cyclic peptide cAA binds to CYP134A1 in the millimolar range, with a very small effect upon the heme iron environment. Decreasing the size of one of the amino acids of the cyclic dipeptide (cLG and cLP) reduces the binding constant by an order of magnitude and the percentage spin shift at least 4-fold, with the smaller side chain glycine exhibiting looser binding. The polarity of the compound is also not the only factor in affecting binding to CYP134A1, with the equally nonpolar cVV dipeptide binding five times more weakly than cLL and exhibiting only 50% of the spin state shift seen for cLL. This suggests that the active site is carefully tuned to receive the side chains of the cLL peptide, a proposition supported by the weakened binding of cMM, which has longer side chains on both positions than cLL. Interestingly, cLF binds twice as tightly as cLL and exhibits the same effect on the heme iron environment, suggesting that there would be no preference for cLL oxidation should cLF be present in the cell. In this regard, the system is limited to the binding constraints available to it in terms of size and polarity of the alkyl side chains, with the isobutyl and benzyl side chains difficult to distinguish for CYP134A1. The importance of one leucyl side chain can also be seen in the binding of cLW, which exhibits very tight binding although a limited spin state change. Combining the binding information of the cyclic dipeptides, it appears that one leucyl chain is important for substrate recognition, while the second side chain should also be a moderately large hydrophobic group. It would appear as though the displacement of the heme-bound water molecule, and thus a change in spin state, depends closely upon the size of this second substituent.

Other somewhat simplified substrates were tested for binding to CYP134A1, with both dimethylpyrazine and tetramethylpyrazine failing to illicit any change in the environment of the heme iron, most likely due to the small size of the side chains on the ring. Quinone and hydroxyquinone compounds bearing two *tert*-butyl groups both bind to CYP134A1, with the quinone form binding more tightly and eliciting the largest effect upon the heme iron environment. It is possible that the difference observed in binding is due to the difference in the carbonyl and alcohol ring substituents, as the overall geometry of the two compounds should be very similar. The binding of phenyl-substituted imidazoles to CYP134A1 was also determined, with 2-phenylimidazole the weakest binding and exhibiting a type 1 spectrum, while 1-phenylimidazole and 4-phenylimidazole bound more tightly, displaying type 2 spectra, indicating nitrogen coordination to the heme iron. 1- and 4-phenylimidazole compounds exhibited around half of the effect on the heme iron environment that was seen with imidazole (the substrate exhibiting the highest substrate-bound Soret absorption values for type 2 binding), while 2-phenylimidazole exhibited around half of the effect on the heme iron environment compared to cLL. This possibly indicates equilibrium between open and closed forms of CYP134A1 in solution, where the closed form binds such phenylimidazole compounds in a manner seen in the crystal structures.

Substrate Oxidation by CYP134A1. The oxidation of cLL by wild-type CYP134A1 indicates that CYP134A1 is capable of accepting electrons from several different ferredoxin electron transfer proteins with varying levels of efficiency, as seen in the differing levels of product formation observed (Table 3). The product was identified by analysis of the observed mass spectral properties with comparison to the mass spectra of cLL (Figure 4). Derivatization (methylation) of the isolated reaction products with TMSH was necessary to observe the product by GCMS (SI Figure 2), as treatment with silylating or acetylating reagents failing to afford any visible product peak that was distinguishable from the large starting material peak. Treatment of the cLL starting material with TMSH indicated small levels of the methylated phenol tautomer of cLL, with an increased mass of the cLL base peak (m/z 170) by 14 mass units due to the addition of a CH₂ group (m/z 184). The base peak in all cyclic peptides is due to the elimination of the alkyl side chain, a feature seen for all cyclic dipeptide alkyl side chains larger than methyl (proline is an exception due to the ring structure of the side chain). The product peak has a base peak of m/z 200, indicating addition of an oxygen atom to the methylated phenol tautomer of cLL. This base peak also corresponds to that expected for pulcherriminic acid, although as this peak is only visible after methylation, the product would appear to be more likely a methylated phenol tautomer of cLL bearing an additional oxygen atom. The position of the oxygen is not clearly assignable without authentic synthetic standards, with products containing either a carbon-centered hydroxyl group or an *N*-oxide being possible. The lack of a mass spectral peak corresponding to that of an aromatized diketopiperazine ring through the elimination of water, however, does favor an *N*-oxide type structure.

The oxidation of cLF by CYP134A1 also generates a product that appears to be comparable to that seen for cLL (a methylated phenol tautomer of cLF bearing an additional oxygen atom), with a similar alteration in base peaks observed for this product (SI Figure 3). The product of cMM oxidation by CYP134A1 does not seem to follow the same pattern seen for the other substrates; rather the product corresponds to an aromatized ring

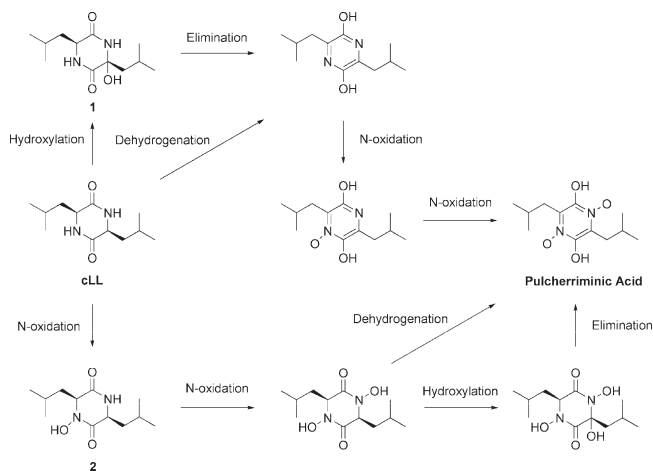


FIGURE 5: Possible oxidation pathways for the formation of pulcherriminic acid from cLL catalyzed by CYP134A1 oxidation, with the possible products isolated from *in vitro* turnover experiments in this work indicated by **1** and **2**.

with both phenol oxygens methylated (SI Figure 4). This is not present in the control reactions, which only exhibit methylated phenol tautomers of cMM in a similar manner as observed for cLL and cLF. The aromatized product suggests a different mechanism in operation for cMM compared to the substrate cLL and close analogue cLF, involving either carbon hydroxylation and concomitant elimination or dehydrogenation of the diketopiperazine ring. Identification of this product does indicate that CYP134A1 is capable of catalyzing chemistry to aromatize the diketopiperazine ring, although it appears as though this is not the primary oxidative route of cLL catalyzed by CYP134A1 *in vitro*.

Mechanistic Possibilities for CYP134A1-Catalyzed Oxidation. The oxidation of the cLL substrate to the final product pulcherriminic acid can be thought of as a three-step oxidative process, with dehydrogenation of the ring forming an aromatic system and two N-oxidations (Figure 5). The order of the steps is unclear, with the dehydrogenation possible via either direct dehydrogenation of the ring following initial formation of a carbon centered radical and electron transfer, through initial hydroxylation and then elimination of water or via a one-electron oxidation of a nitrogen ring atom, followed by deprotonation of the adjacent C–H group and then final electron transfer to the heme to afford the dehydrated product. The N-oxidation mechanism most likely occurs via initial electron abstraction from the nitrogen atom followed by oxygen rebound. There is also the possibility that the final pulcherriminic acid structure is formed by nonenzymatically catalyzed oxidation of a product of CYP134A1 oxidation following release into the extracellular medium, a hypothesis that is supported to some extent by the isolation of a singly oxygenated cLL product from CYP134A1 *in vitro* turnover. The isolation of an aromatized product in the case of cMM oxidation indicates that aromatization of the diketopiperazine ring is able to be performed by CYP134A1, although it would appear from the *in vitro* turnovers of cLL and cLF that initial nitrogen atom oxidation would occur first.

Catalytic Residues Suggest an Unusual Route to Oxygen Protonation. While the overall structure of CYP134A1 does not differ widely from the closest structurally related P450s (with the exception of the B–B₂ loop region), one factor that makes CYP134A1 most interesting from a mechanistic perspective is the alteration of the typically highly conserved I-helix

acid/alcohol pair responsible for the correct protonation of reactive intermediates in the P450 active cycle (68). The lack of an alcohol residue in CYP134A1 and its replacement with Pro-237 make CYP134A1 one of a small group of P450s that do not possess the normal hydrogen-bonding residue at this position. The most widely studied member of this group is EryF, which is still able to catalyze hydroxylation chemistry due to the involvement of a hydroxyl group present in the substrate that assists in forming the hydrogen-bonding network normally orchestrated with the conserved alcohol residue in the I-helix (66). This type of substrate-mediated recovery of intermediate protonation alleviates the effects normally observed by mutation of the alcohol residue, which include high levels of uncoupling (direction of electrons into noncatalytically profitable pathways) and exemplified by high levels of hydrogen peroxide formation rather than substrate hydroxylation (69–74). These types of mutations have been widely used to study the effect of normally minor oxidation pathways involving nonferryl intermediates in the P450 activation cycle, including the ferric peroxy anion and the ferric hydroperoxy species. These intermediates, while not as powerful as the ferryl species in terms of oxidative potential, are believed to play roles in energetically less demanding reactions in some cases (3, 75). The ferric peroxy species is involved in the oxidative decarboxylation of aldehydes (76–78), while the hydroperoxy species possibly catalyzes the oxidation of heteroatoms (79–81) or epoxidation of alkenes (82, 83). The possibility of the cLL substrate carbonyl oxygen or ring nitrogen forming the same type of H-bonding pattern in CYP134A1 to that seen for EryF would require a rearrangement of the active site upon substrate binding and a highly ordered active site water network to allow a similar type of cLL binding as seen in the EryF substrate. An alternate explanation would invoke the use of the hydroperoxy species as an oxidant. However, it is unclear whether this species would be a powerful enough to catalyze the oxidation of the diketopiperazine ring nitrogen atoms in cLL.

The presence of the Pro-237 residue in the CYP134A1 active site has another potential mechanistic explanation, with such a residue found in the active site of the *B. subtilis* fatty acid peroxidase Bs β (Pro-243), albeit with differences in the relative positioning of the I-helix to the heme compared to CYP134A1 (61). This enzyme is able to efficiently and rapidly oxidize fatty acids close to the carboxyl group using hydrogen peroxide, rather than activating molecular oxygen. This type of reaction no longer requires the binding of molecular oxygen to the heme iron and the delivery of electrons from ancillary redox partner proteins; rather the enzyme uses a “short-cut” known as the peroxide shunt pathway to afford the reactive intermediate immediately preceding the ferryl species. This process allows oxidation to be catalyzed at a much higher rate than normal oxygen activation, with the bound substrate carboxyl group likely to be responsible for the generation of the ferryl species from the initial hydrogen peroxide bound heme, itself held in place by salt bridges formed from the preceding Bs β residue Arg-242. The likelihood of peroxidase activity in the case of CYP134A1 appears to be low, as peroxide does not afford product as seen with the redox partner electron transfer systems, although the measured pH of the reactions were the same as reported for Bs β oxidation of polycyclic aromatic compounds (84).

Does the C-Terminal Loop Extension Regulate Electron Transfer in CYP134A1? An additional consideration with the oxygen activation mechanism utilized by CYP134A1 is the role of the 332–341 residue loop extension prior to the heme iron ligated

cysteine residue on the proximal side of the heme group. This region of P450s has been shown to be involved in the transfer of electrons to the heme group from ancillary redox proteins, a process necessary in oxygen activation from molecular oxygen. The interaction site of redox proteins with P450s has been demonstrated for P450_{BM3} (85) and modeled for P450_{cam} (86), with both studies implicating a region of interaction essentially on the site where the CYP134A1 loop extension occurs. The presence of this loop in CYP134A1 is most unusual for a P450, with few other P450s (apart from CYP134A1 homologues) exhibiting a similar region in sequence alignments. Examples of mechanistically unrelated P450s with similar loops are found with the CYP74 subfamily (87), which catalyze the rearrangement of alkyl hydroperoxides rather than oxygenase chemistry (88), and the CYP24 subfamily, mitochondrial P450s responsible for vitamin D oxidation (89). The CYP24A1 loop is believed to interact with the redox partner protein Adx (90), although the CYP134A1 loop does not contain the same concentration of lysine residues (89). As CYP134A1 does not have a coexpressed ferredoxin, electrons would have to be transferred from one of the endogenous ferredoxin proteins present in *B. subtilis*. Several such ferredoxins have been identified and have been shown to be able to support electron transport to P450_{BioI}, albeit at a low rate (91, 92). The effect of this loop on the electrostatic potential of the redox partner interaction surface is not marked, with the electrostatic potential of this region still dominated by positive charge, albeit with the presence of more hydrophobic residues (SI Figure 7). The exact purpose of this loop in CYP134A1 is therefore unclear, although its position does suggest that it is involved in moderating interaction with redox partner proteins for CYP134A1. A peroxygenase function of CYP134A1 would imply that this loop would prevent interaction with endogenous electron transfer partners, which is not supported by the *in vitro* turnover experiments.

Conclusions. P450 CypX (CYP134A1) from *B. subtilis* has been shown to bind the diketopiperazine cLL, the postulated *in vivo* substrate for CYP134A1, with low micromolar affinity. Other cyclic dipeptides with similar alkyl side chains to cLL bind with comparable tightness to CYP134A1, although the selectivity of the preceding cyclodipeptide synthase in the pulcherriminic acid operon of *B. subtilis* for formation of cLL eliminates the need for P450-mediated selectivity for cLL. Turnover of cLL by CYP134A1 is supported by several *in vitro* electron transfer partners, with the product of oxidation appearing to correspond to a singly oxidized cLL product rather than the expected final product of CYP134A1, pulcherriminic acid. The oxidation of substrates similar to cLL reveals that different oxidative pathways exist for CYP134A1 diketopiperazine oxidation, with the exact mechanism of CYP134A1 *in vivo* oxidation requiring further study. The crystal structure of CYP134A1 has revealed a nonpolar active site containing an unusual proline residue in the place of the normally conserved alcohol residue responsible for oxygen activation. The B–B₂ loop has been shown to exist in multiple conformations, one of which is likely to correspond to the substrate-free active site conformation in solution. Future studies will characterize the products of oxidation of CYP134A1 to shed more light on the chemical mechanism of this unusual oxidation.

ACKNOWLEDGMENT

The authors thank Luet-Lok Wong (Inorganic Chemistry Laboratory, Oxford University, U.K.) for provision of the redox

partner proteins, Jessica Staaden and Anna Scherer for support with crystallization, Nicolas Werbeck and Hannes Mutschler for discussions concerning substrate binding, Anton Meinhart and Daniel Frey for assistance with crystallographic computer packages, and Robert Shoeman and Melanie Müller for mass spectral analyses. We thank Ingrid Vetter for support of the crystallographic software and Chris Roome for IT support. Diffraction data were collected at the Swiss Light Source, beamline X10SA, Paul Scherrer Institute, Villigen, Switzerland. We thank the Dortmund-Heidelberg team for data collection and the PXII staff for their support in setting up the beamline.

SUPPORTING INFORMATION AVAILABLE

Binding curves for cLL, cLF, cMM, cVV, 2,5-di-*tert*-butylhydroxyquinone, and 2,5-di-*tert*-butylquinone substrates to CYP134A1; retention times and major MS fragmentation peaks for cLL, cLF, and cMM together with compounds present in the GCMS analysis of the CYP134A1 turnover experiments; GC traces of CYP134A1-catalyzed turnover of cLL, cLF, and cMM substrates; list of *Bacillus subtilis* P450s; structural comparisons of known P450 structures with similarity to CYP134A1; substrate recognition site (SRS) alignment of P450s with high SRS homology to CYP134A1; P450s with homology to CYP134A1 but significant alterations in critical structural elements; MS fragmentation analyses of cLF/cMM and oxidized cLF/cMM products; optimal cLL docking solutions obtained from Autodock and Pathdock; surface charge comparison on the proximal side of the heme group in various cytochrome P450s. This material is available free of charge via the Internet at <http://pubs.acs.org>.

REFERENCES

- Ortiz de Montellano, P. R. (2008) Cytochrome P450: Structure, Mechanism and Biochemistry, 3rd ed., Springer-Verlag, New York.
- Cryle, M. J., Stok, J. E., and De Voss, J. J. (2003) Reactions catalyzed by bacterial cytochromes P450. *Aust. J. Chem.* 56, 749–762.
- Ortiz De Montellano, P. R., and De Voss, J. J. (2002) Oxidizing species in the mechanism of cytochrome P450. *Nat. Prod. Rep.* 19, 477–493.
- Denisov, I. G., Makris, T. M., Sligar, S. G., and Schlichting, I. (2005) Structure and chemistry of cytochrome P450. *Chem. Rev.* 105, 2253–2278.
- Hlavica, P. (2002) N-oxidative transformation of free and N-substituted amine functions by cytochrome P450 as means of bioactivation and detoxication. *Drug Metab. Rev.* 34, 451–477.
- Ortiz de Montellano, P. R., and De Voss, J. J. (2008) Substrate oxidation by cytochrome P450 enzymes, in *Cytochrome P450: Structure, Mechanism and Biochemistry* (Ortiz de Montellano, P. R., Ed.) p 689, Springer-Verlag, New York.
- Kelly, W. L., and Townsend, C. A. (2002) Role of the cytochrome P450 NocL in nocardicin A biosynthesis. *J. Am. Chem. Soc.* 124, 8186–8187.
- Naur, P., Petersen, B. L., Mikkelsen, M. D., Bak, S., Rasmussen, H., Olsen, C. E., and Halkier, B. A. (2003) CYP83A1 and CYP83B1, two nonredundant cytochrome P450 enzymes metabolizing oximes in the biosynthesis of glucosinolates in *Arabidopsis*. *Plant Physiol.* 133, 63–72.
- Mikkelsen, M. D., Petersen, B. L., Olsen, C. E., and Halkier, B. A. (2002) Biosynthesis and metabolic engineering of glucosinolates. *Amino Acids* 22, 279–295.
- Nielsen, J. S., and Moller, B. L. (2000) Cloning and expression of cytochrome P450 enzymes catalyzing the conversion of tyrosine to p-hydroxyphenylacetaldoxime in the biosynthesis of cyanogenic glucosides in *Triglochin maritima*. *Plant Physiol.* 122, 1311–1321.
- Koch, B. M., Sibbesen, O., Halkier, B. A., Svendsen, I., and Moeller, B. L. (1995) The primary sequence of cytochrome P450_{tyr}, the multifunctional N-hydroxylase catalyzing the conversion of L-tyrosine to p-hydroxyphenylacetaldehyde oxime in the biosynthesis of the cyanogenic glucoside dhurrin in *Sorghum bicolor* (L.) Moench. *Arch. Biochem. Biophys.* 323, 177–186.

12. Halkier, B. A., Nielsen, H. L., Koch, B., and Moeller, B. L. (1995) Purification and characterization of recombinant cytochrome P450TYR expressed at high levels in *Escherichia coli*. *Arch. Biochem. Biophys.* 322, 369–377.
13. Gondry, M., Sauguet, L., Belin, P., Thai, R., Amouroux, R., Tellier, C., Tuphile, K., Jacquet, M., Braud, S., Courcon, M., Masson, C., Dubois, S., Lautru, S., Lecoq, A., Hashimoto, S.-i., Genet, R., and Pernodet, J.-L. (2009) Cyclodipeptide synthases are a family of tRNA-dependent peptide bond-forming enzymes. *Nat. Chem. Biol.* 5, 414–420.
14. Uffen, R. L., and Canale-Parola, E. (1972) Synthesis of pulcherriminic acid by *Bacillus subtilis*. *J. Bacteriol.* 111, 86–93.
15. Tang, M. R., Sternberg, D., Behr, R. K., Sloma, A., and Berka, R. M. (2006) Use of transcriptional profiling and bioinformatics to solve production problems: Eliminating red pigment production in a *Bacillus subtilis* strain producing hyaluronic acid. *Ind. Biotechnol.* 2, 66–74.
16. Uffen, R. L., and Canale-Parola, E. (1969) Isolation of pulcherriminic acid from cultures of *Bacillus cereus*. *Z. Allg. Mikrobiol.* 9, 231–233.
17. MacDonald, J. C. (1967) Isolation of pulcherriminic acid from *Bacillus cereus*. *Can. J. Microbiol.* 13, 17–20.
18. MacDonald, J. C. (1966) The isolation of pulcherriminic acid from *Micrococcus violagabriellae*. *Can. J. Microbiol.* 12, 55–59.
19. Campbell, J. N., Nichols, J. L., and Berry, S. A. (1964) Characterization of the pigment of *Micrococcus violagabriellae*. *Can. J. Microbiol.* 10, 659–675.
20. Canale-Parola, E. (1963) A red pigment produced by aerobic spore-forming bacteria. *Arch. Mikrobiol.* 46, 414–427.
21. MacDonald, J. C. (1963) The structure of pulcherriminic acid. *Can. J. Chem.* 41, 165–172.
22. Cook, A. H., and Slater, C. A. (1954) Metabolism of wild yeasts. I. Chemical nature of pulcherrimin. *J. Inst. Brewing* 60, 213–217.
23. Kluyver, A. J., van der Walt, J. P., and van Triet, A. J. (1953) Pulcherrimin, the pigment of *Candida pulcherrima*. *Proc. Natl. Acad. Sci. U.S.A.* 39, 583–593.
24. Kupfer, D. G., Uffen, R. L., and Canale-Parola, E. (1967) Role of iron and molecular oxygen in pulcherrimin synthesis by bacteria. *Arch. Mikrobiol.* 56, 9–21.
25. Neilands, J. (1967) Hydroxamic acids in nature. *Science (Washington, DC)* 156, 1443–1447.
26. Furuya, T., Nishi, T., Shibata, D., Suzuki, H., Ohta, D., and Kino, K. (2008) Characterization of orphan monooxygenases by rapid substrate screening using FT-ICR mass spectrometry. *Chemistry & Biology* 15, 563–572.
27. Furuya, T., Shibata, D., and Kino, K. (2009) Phylogenetic analysis of *Bacillus* P450 monooxygenases and evaluation of their activity towards steroids. *Steroids* 74, 906–912.
28. Bradford, M. M. (1976) A rapid and sensitive method for quantitation of microgram quantities of protein utilizing the principle of protein-dye-binding. *Anal. Biochem.* 72, 248–254.
29. Yu, C. A., Gunsalus, I. C., Katagiri, M., Suhara, K., and Takemori, S. (1974) Cytochrome P-450cam. *J. Biol. Chem.* 249, 94–101.
30. Dawson, J. H., Andersson, L. A., and Sono, M. (1982) Spectroscopic investigations of ferric cytochrome P-450-CAM ligand complexes. Identification of the ligand trans to cysteinate in the native enzyme. *J. Biol. Chem.* 257, 3606–3617.
31. Peterson, J. A., Lu, J. Y., Geisselsoder, J., Graham-Lorence, S., Carmona, C., Witney, F., and Lorence, M. C. (1992) Cytochrome P-450terp. Isolation and purification of the protein and cloning and sequencing of its operon. *J. Biol. Chem.* 267, 14193–14203.
32. Bell, S. G., Xu, F., Johnson, E. O. D., Forward, I. M., Bartlam, M., Rao, Z., and Wong, L.-L. (2010) Protein recognition in ferredoxin-P450 electron transfer in the class I CYP199A2 system from *Rhodospirillum rubrum*. *J. Biol. Inorg. Chem.* 15, 315–328.
33. Bell, S. G., Dale, A., Rees, N. H., and Wong, L.-L. (2010) A cytochrome P450 class I electron transfer system from *Novosphingobium aromaticivorans*. *Appl. Microbiol. Biotechnol.* 86, 163–175.
34. Bell, S., Tan, A., Johnson, E., and Wong, L. (2010) Selective oxidative demethylation of veratric acid to vanillic acid by CYP199A4 from *Rhodospirillum rubrum*. *Mol. Biosystems* 6, 206–214.
35. Kabsch, W. (1993) Automatic processing of rotation diffraction data from crystals of initially unknown symmetry and cell constants. *J. Appl. Crystallogr.* 26, 795–800.
36. Vonrhein, C., Blanc, E., Roversi, P., and Bricogne, G. (2007) Automated structure solution with autoSHARP, in *Macromolecular Crystallography Protocols* (Doublié, S., Ed.) pp 215–230, Humana Press, Totowa, NJ.
37. Emsley, P., Lohkamp, B., Scott, W. G., and Cowtan, K. (2010) Features and development of Coot. *Acta Crystallogr., Sect. D: Biol. Crystallogr.* 66, 486–516.
38. Brunger, A. T., Adams, P. D., Clore, G. M., DeLano, W. L., Gros, P., Grosse-Kunstleve, R. W., Jiang, J.-S., Kuszewski, J., Nilges, M., Pannu, N. S., Read, R. J., Rice, L. M., Simonson, T., and Warren, G. L. (1998) Crystallography & NMR System: A new software suite for macromolecular structure determination. *Acta Crystallogr., Sect. D: Biol. Crystallogr.* 54, 905–921.
39. Murshudov, G. N., Vagin, A. A., and Dodson, E. J. (1997) Refinement of macromolecular structures by the maximum-likelihood method. *Acta Crystallogr., Sect. D: Biol. Crystallogr.* 53, 240–255.
40. Winn, M. D., Isupov, M. N., and Murshudov, G. N. (2001) Use of TLS parameters to model anisotropic displacements in macromolecular refinement. *Acta Crystallogr., Sect. D: Biol. Crystallogr.* 57, 122–133.
41. Painter, J., and Merritt, E. A. (2006) Optimal description of a protein structure in terms of multiple groups undergoing TLS motion. *Acta Crystallogr., Sect. D: Biol. Crystallogr.* 62, 439–450.
42. Painter, J., and Merritt, E. A. (2006) TLSMD web server for the generation of multi-group TLS models. *J. Appl. Crystallogr.* 39, 109–111.
43. Davis, I. W., Leaver-Fay, A., Chen, V. B., Block, J. N., Kapral, G. J., Wang, X., Murray, L. W., III, W., B. A., Snoeyink, J., Richardson, J. S., and Richardson, D. C. (2007) MolProbity: All-atom contacts and structure validation for proteins and nucleic acids. *Nucleic Acids Res.* 35, W375–W383.
44. Laskowski, R. A., MacArthur, M. W., Moss, D. S., and Thornton, J. M. (1993) PROCHECK: A program to check the stereochemical quality of protein structures. *J. Appl. Crystallogr.* 26, 283–291.
45. Krissinel, E., and Henrick, K. (2004) Secondary-structure matching (SSM), a new tool for fast protein structure alignment in three dimensions. *Acta Crystallogr., Sect. D: Biol. Crystallogr.* 60, 2256–2268.
46. Carter, P., Andersen, C., and Rost, B. (2003) DSSPcont: Continuous secondary structure assignments for proteins. *Nucleic Acids Res.* 31, 3293–3295.
47. Holm, L., and Park, J. (2000) DaliLite workbench for protein structure comparison. *Bioinformatics* 16, 566–567.
48. DeLano, W. L. (2002) DeLano Scientific, Palo Alto, CA.
49. Baker, N. A., Sept, D., Joseph, S., Holst, M. J., and McCammon, J. A. (2001) Electrostatics of nanosystems: Application to microtubules and the ribosome. *Proc. Natl. Acad. Sci. U.S.A.* 98, 10037–10041.
50. Morris, G. M., Goodsell, D. S., Halliday, R. S., Huey, R., Hart, W. E., Belew, R. K., and Olson, A. J. (1998) Automated docking using a Lamarckian genetic algorithm and empirical binding free energy function. *J. Comput. Chem.* 19, 1639–1662.
51. Schneidman-Duhovny, D., Inbar, Y., Nussinov, R., and Wolfson, H. J. (2005) PatchDock and SymmDock: Servers for rigid and symmetric docking. *Nucleic Acids Res.* 33, W363–367.
52. Larkin, M. A., Blackshields, G., Brown, N. P., Chenna, R., McGettigan, P. A., McWilliam, H., Valentin, F., Wallace, I. M., Wilm, A., Lopez, R., Thompson, J. D., Gibson, T. J., and Higgins, D. G. (2007) ClustalW and ClustalX version 2. *Bioinformatics* 23, 2947–2948.
53. Altschul, S. F., Madden, T. L., Schaffer, A. A., Zhang, J., Zhang, Z., Miller, W., and Lipman, D. J. (1997) Gapped BLAST and PSI-BLAST: A new generation of protein database search programs. *Nucleic Acids Res.* 25, 3389–3402.
54. Gastegger, E., Gattiker, A., Hoogland, C., Ivanyi, I., Appel, R. D., and Bairoch, A. (2003) ExPASy: The proteomics server for in-depth protein knowledge and analysis. *Nucleic Acids Res.* 31, 3784–3788.
55. McCoy, J. G., Johnson, H. D., Singh, S., Bingman, C. A., Lei, I.-K., Thorson, J. S., and Phillips, G. N., Jr. (2009) Structural characterization of CalO2: A putative orsellinic acid P450 oxidase in the calicheamicin biosynthetic pathway. *Proteins: Struct., Funct., Bioinf.* 74, 50–60.
56. Cryle, M. J., and Schlichting, I. (2008) Structural insights from a P450 carrier protein complex reveal how specificity is achieved in the P450Biol ACP complex. *Proc. Natl. Acad. Sci. U.S.A.* 105, 15696–15701.
57. Cupp-Vickery, J. R., and Poulos, T. L. (1995) Structure of cytochrome P450eryF involved in erythromycin biosynthesis. *Nat. Struct. Biol.* 2, 144–153.
58. Savino, C., Montemiglio, L. C., Sciara, G., Miele, A. E., Kendrew, S. G., Jemth, P., Gianni, S., and Vallone, B. (2009) Investigating the structural plasticity of a cytochrome P450: Three-dimensional structures of P450 EryK and binding to its physiological substrate. *J. Biol. Chem.* 284, 29170–29179.
59. Nagano, S., Li, H., Shimizu, H., Nishida, C., Ogura, H., Ortiz de Montellano, P. R., and Poulos, T. L. (2003) Crystal structures of epothilone D-bound, epothilone B-bound, and substrate-free forms of cytochrome P450epoK. *J. Biol. Chem.* 278, 44886–44893.

60. Matsunaga, I., Ueda, A., Fujiwara, N., Sumimoto, T., and Ichihara, K. (1999) Characterization of the ybdT gene product of *Bacillus subtilis*: Novel fatty acid beta-hydroxylating cytochrome P450. *Lipids* 34, 841–846.
61. Lee, D.-S., Yamada, A., Sugimoto, H., Matsunaga, I., Ogura, H., Ichihara, K., Adachi, S.-i., Park, S.-Y., and Shiro, Y. (2003) Substrate recognition and molecular mechanism of fatty acid hydroxylation by cytochrome P450 from *Bacillus subtilis*. *J. Biol. Chem.* 278, 9761–9767.
62. Sabbadin, F., Jackson, R., Haider, K., Tampi, G., Turkenburg, J. P., Hart, S., Bruce, N. C., and Grogan, G. (2009) The 1.5-Å structure of XplA-heme, an unusual cytochrome P450 heme domain that catalyzes reductive biotransformation of royal demolition explosive. *J. Biol. Chem.* 284, 28467–28475.
63. Cryle, M. J., and De Voss, J. J. (2004) Carbon-carbon bond cleavage by cytochrome P450BioI (CYP107H1). *Chem. Commun.*, 86–87.
64. Cryle, M. J., Matovic, N. J., and De Voss, J. J. (2003) Products of cytochrome P450BioI (CYP107H1)-catalyzed oxidation of fatty acids. *Org. Lett.* 5, 3341–3344.
65. Stok, J. E., and De Voss, J. J. (2000) Expression, purification, and characterization of BioI: A carbon-carbon bond cleaving cytochrome P450 involved in biotin biosynthesis in *Bacillus subtilis*. *Arch. Biochem. Biophys.* 384, 351–360.
66. Cupp-Vickery, J. R., Han, O., Hutchinson, R., and Poulos, T. L. (1996) Substrate-assisted catalysis in cytochrome P450eryF. *Nat. Struct. Biol.* 3, 632–637.
67. Berlin, P., Le Du, M. H., Fielding, A., Lequin, O., Jacquet, M., Charbonnier, J.-B., Lecoq, A., Thai, R., Courcon, M., Masson, C., Dugave, C., Genet, R., Pernodet, J.-L., and Gondry, M. (2009) Identification and structural basis of the reaction catalyzed by CYP121, an essential cytochrome P450 in *Mycobacterium tuberculosis*. *Proc. Natl. Acad. Sci. U.S.A.* 106, 7426–7431.
68. von Koenig, K., and Schlichting, I. (2007) Cytochromes P450—Structural basis for binding and catalysis. *Metal Ions Life Sci.* 3, 235–265.
69. Truan, G., and Peterson, J. A. (1998) Thr268 in substrate binding and catalysis in P450BM-3. *Arch. Biochem. Biophys.* 349, 53–64.
70. Yeom, H., Sligar, S. G., Li, H., Poulos, T. L., and Fulco, A. J. (1995) The role of Thr268 in oxygen activation of cytochrome P450BM-3. *Biochemistry* 34, 14733–14740.
71. Kimata, Y., Shimada, H., Hirose, T., and Ishimura, Y. (1995) Role of Thr-252 in cytochrome P450CAM: A study with unnatural amino acid mutagenesis. *Biochem. Biophys. Res. Commun.* 208, 96–102.
72. Imai, M., Shimada, H., Watanabe, Y., Matsushima-Hibiya, Y., Makino, R., Koga, H., Horiuchi, T., and Ishimura, Y. (1989) Uncoupling of the cytochrome P-450cam monooxygenase reaction by a single mutation, threonine-252 to alanine or valine: A possible role of the hydroxy amino acid in oxygen activation. *Proc. Natl. Acad. Sci. U.S.A.* 86, 7823–7827.
73. Martinis, S. A., Atkins, W. M., Stayton, P. S., and Sligar, S. G. (1989) A conserved residue of cytochrome P-450 is involved in heme-oxygen stability and activation. *J. Am. Chem. Soc.* 111, 9252–9253.
74. Cryle, M. J., and De Voss, J. J. (2008) The role of the conserved threonine in P450BM3 oxygen activation: Substrate-determined hydroxylation activity of the Thr268Ala mutant. *ChemBioChem* 9, 261–266.
75. Hlavica, P. (2004) Models and mechanisms of O-O bond activation by cytochrome P450. A critical assessment of the potential role of multiple active intermediates in oxidative catalysis. *Eur. J. Biochem.* 271, 4335–4360.
76. Shyadehi, A. Z., Lamb, D. C., Kelly, S. L., Kelly, D. E., Schunck, W.-H., Wright, J. N., Corina, D., and Akhtar, M. (1996) The mechanism of the acyl-carbon bond cleavage reaction catalyzed by recombinant sterol 14-demethylase of *Candida albicans* (other names are: lanosterol 14-demethylase, P-450, and CYP51). *J. Biol. Chem.* 271, 12445–12450.
77. Kao, Y.-C., Korzekwa, K. R., Laughton, C. A., and Chen, S. (2001) Evaluation of the mechanism of aromatase cytochrome P450. A site-directed mutagenesis study. *Eur. J. Biochem.* 268, 243–251.
78. Oh, S. S., and Robinson, C. H. (1993) Mechanism of human placental aromatase: A new active site model. *J. Steroid Biochem. Mol. Biol.* 44, 389–397.
79. Guengerich, F. P., Vaz, A. D. N., Raner, G. N., Pernecky, S. J., and Coon, M. J. (1997) Evidence for a role of a perferryl-oxygen complex, FeO_3^+ , in the N-oxygenation of amines by cytochrome P450 enzymes. *Mol. Pharmacol.* 51, 147–151.
80. Volz, T. J., Rock, D. A., and Jones, J. P. (2002) Evidence for two different active oxygen species in cytochrome P450 BM3 mediated sulfoxidation and N-dealkylation reactions. *J. Am. Chem. Soc.* 124, 9724–9725.
81. Cryle, M. J., and De Voss, J. J. (2006) Is the ferric hydroperoxy species responsible for sulfur oxidation in cytochrome P450s? *Angew. Chem., Int. Ed.* 45, 8221–8223.
82. Vaz, A. D. N., McGinnity, D. F., and Coon, M. J. (1998) Epoxidation of olefins by cytochrome P450: Evidence from site-specific mutagenesis for hydroperoxy-iron as an electrophilic oxidant. *Proc. Natl. Acad. Sci. U.S.A.* 95, 3555–3560.
83. Jin, S., Makris, T. M., Bryson, T. A., Sligar, S. G., and Dawson, J. H. (2003) Epoxidation of olefins by hydroperoxy-ferric cytochrome P450. *J. Am. Chem. Soc.* 125, 3406–3407.
84. Torres, E., Hayen, H., and Niemeyer, C. M. (2007) Evaluation of cytochrome P450BSb reactivity against polycyclic aromatic hydrocarbons and drugs. *Biochem. Biophys. Res. Commun.* 355, 286–293.
85. Sevrionkova, I. F., Li, H., Zhang, H., Peterson, J. A., and Poulos, T. L. (1999) Structure of a cytochrome P450-redox partner electron-transfer complex. *Proc. Natl. Acad. Sci. U.S.A.* 96, 1863–1868.
86. Pochapsky, T. C., Lyons, T. A., Kazanis, S., Arakaki, T., and Ratnaswamy, G. (1996) A structure-based model for cytochrome P450cam-putidaredoxin interactions. *Biochimie* 78, 723–733.
87. Lee, D., Nioche, P., Hamberg, M., and Raman, C. (2008) Structural insights into the evolutionary paths of oxylipin biosynthetic enzymes. *Nature* 455, 363–368.
88. Grechkin, A. N. (2002) Hydroperoxide lyase and divinyl ether synthase. *Prostaglandins Other Lipid Mediat.* 68–69, 457–470.
89. Annalora, A. J., Goodin, D. B., Hong, W.-X., Zhang, Q., Johnson, E. F., and Stout, C. D. (2010) Crystal structure of CYP24A1, a mitochondrial cytochrome P450 involved in vitamin D metabolism. *J. Mol. Biol.* 396, 441–451.
90. Asya, V. G., Frank, H., Burkhard, S., Jürgen, M., Udo, H., and Rita, B. (2000) Adrenodoxin: Structure, stability, and electron transfer properties. *Proteins: Struct., Funct., Genet.* 40, 590–612.
91. Green, A. J., Munro, A. W., Cheesman, M. R., Reid, G. A., von Wachenfeldt, C., and Chapman, S. K. (2003) Expression, purification and characterisation of a *Bacillus subtilis* ferredoxin: A potential electron transfer donor to cytochrome P450 BioI. *J. Inorg. Biochem.* 93, 92–99.
92. Lawson, R. J., von Wachenfeldt, C., Haq, I., Perkins, J., and Munro, A. W. (2004) Expression and characterization of the two flavodoxin proteins of *Bacillus subtilis*, YkuN and YkuP: Biophysical properties and interactions with cytochrome P450 BioI. *Biochemistry* 43, 12390–12409.